

FOURTH SEMIANNUAL REPORT

NASA Grant NGR-05-009-030

Physical Processes in the
Magneto-Plasmadynamic Arc

May 1968

R. Lovberg, Principal Investigator
University of California, San Diego
La Jolla, California

Introduction

This report will summarize the work performed under NASA Grant NGR-05-009-030 during its two year period (March 1966-March 1968), although most of what is discussed here in detail will cover the last semiannual period (September 1967-March 1968).

I. Summary of Overall Program

The work done under this grant is a series of experiments directed toward a fundamental understanding of the Magneto-plasmadynamic arc. The main emphasis has been on the behavior of the arc itself within its region of current flow, rather than on the properties of the expelled plasma (although recent experiments have been done in this area), and no attention at all has so far been given to the thrust or efficiency which might characterize the system.

The motive for studies of the internal physics of the MPD arc is simply that this system (as defined by its characteristic mass flow rate, magnetic bias field, and geometry) has been found to be significantly more efficient than any other form of arc in converting electrical input power into directed propellant kinetic energy (1-5). The bulk of MPD research effort has, quite reasonably, been concerned with optimization of the arc for propulsion use, which implies an emphasis on thrust, specific impulse, and most importantly, efficiency. Since these parameters can be determined by measurements external to the arc itself, there has been no compelling reason, at least from the application point of view, for determining the precise internal character of the discharge.

An even more effective inhibition against internal experiments on the MPD arc is the very high power density in the current channel. Even a

relatively small system consumes several kilowatts of electrical power in a volume of no more than a few cubic centimeters; this environment is quite destructive to any kind of a probe which might be placed in it. The physical dimensions of the discharge region in a typical arc are also small enough to make the achievement of good spatial resolution quite difficult in those experiments (e.g., optical spectroscopy) which might otherwise be feasible.

We have undertaken a program of internal physical measurements of an MPD system in spite of the difficulties mentioned above. The strategy has been to sidestep these troubles by (a) running the arc on short pulses, so that the cumulative heat loading to probes does not destroy them, and (b) making the system with a relatively large and open coaxial electrode structure so that the spatial resolution of the various probes is a relatively small fraction of the interelectrode spacing. Both of these modifications of "standard" operating conditions have been adopted with considerable caution: pulsed operation, for example, is a legitimate approximation to D.C. operation only if a true steady state is achieved for a fair fraction of the pulse time, and a major change in arc geometry might result in entirely atypical behavior of the arc. We have attempted to meet the first objection by employing a pulse length of 500 microseconds. Any characteristic time constant of the arc should be much shorter than this, with the single exception of the thermal time constant of the tungsten cathode, which is several seconds in a normal arc. In the present system, this particular difficulty--attaining a steady-state cathode temperature high enough to supply arc electrons by thermionic emission--has been avoided by a pulsed preheating of the cathode prior to the main arc pulse. For this purpose, our cathode has the form of a U-shaped ribbon of 1 cm x 0.005 in tungsten, through which

several thousand amperes of 60 cps A.C. current are passed for about 0.4 seconds. A temperature of about 3400°K is achieved.

The electrode geometry consists of a 4" diameter stainless steel cylinder which serves as the anode, with the aforementioned tungsten ribbon cathode mounted on its axis and recessed about 3 cm back of the edge of the cylinder. In adopting this geometry, it was decided that if typical MPD arc behavior (in terms of terminal impedance as a function of bias field, for example) could not be obtained, it would then be possible to place various shaped inserts between the anode and cathode until an adequately good approximation to the usual arc configuration is obtained. Fortunately, these measures did not prove necessary.

Propellant flow in this system is also pulsed. In this way, the arc can be operated against a high vacuum environment, rather than the considerable background pressure which necessarily accompanies the typical flow rate into vacuum systems of ordinary capacity.

II. Summary of Earlier Results

The following will briefly summarize our experimental results during the first three semiannual periods of this grant (6,7,8).

1. The pulsed arc was found to be typical of MPD arcs in most of its characteristics. The variation of arc impedance with bias field and the absolute value of impedance itself corresponds to ordinary experience. Our standard operating conditions have been:

Arc voltage 75 volts

Arc current 550 amperes

Bias field 2200 gauss (maximum,
at rear of arc chamber)

Propellant: Argon

Propellant flow rate: ~ 0.02 g/sec

For a given bias field strength, the arc voltage is nearly independent of arc current; however, the voltage increases linearly with bias field.

2. By the use of magnetic field probes and Rogowski current loops it was determined that under standard arc conditions, the actual arc current distribution is not symmetrical, but is highly localized into a "spoke" at one azimuth; this spoke rotates at a frequency which depends upon the product IB (arc current \times bias field), and also the mass flow rate. For a given rate of mass flow, the rotation rate is linear with IB over nearly a factor of ten variation in IB .

3. In its geometrical configuration, the current channel is highly constricted at the electrodes, and flares somewhat in between, mostly in the axial direction. The current appears to emerge from a spot of the order of 1 cm in diameter at the forward edge of the anode, and converge again to the heated tungsten ribbon cathode. There appears to be no azimuthal component in the current spoke. There is, however, evidence for azimuthal current in the anode sheath region.⁸

4. Single and double floating probes have been used to obtain the distribution of potential and electric field within the arc. Such floating potential data are subject to correction for the sheath drop, which is in the neighborhood of 3 or 4 times kT/e . It will be shown later that this correction amounts to about 3 volts, so that the measured potentials do not differ markedly from space potential.

It has been found that the plasma potential distribution is one for which the magnetic bias field lines are, very closely, lines of constant potential. The magnitude of the total potential drop across the main arc channel is only about 45 volts out of the 75 volts applied, with the remaining 30 volts appearing over a thin anode sheath. Approximately 40% of the input electrical power is thus dissipated at the anode, a result which is in agreement with calorimetric measurements of power loss in other MPD arc.

III. Experimental Results for Fourth Semiannual Period

This section summarizes the experimental progress during the last semiannual report period (September 1967 to March 1968).

1. Spectroscopy

A collimated telephoto lens was mounted on a spectrometer making it possible to spatially analyze the radiation from the arc. A spectroscopic survey from 4000 Å to 5010 Å showed the existence of only AII lines. No AI lines were observed. The line intensities emitted from the spoke were an order of magnitude greater than emissions from any other region of the arc or exhaust plume.

The electron temperature of the plasma in the current spoke has been determined by measuring the relative line intensities of thirteen AII spectral lines. The energy levels involved in the transitions are included in a cluster of levels having interlevel gaps of less than an electron volt, therefore the population densities of these levels should be in local thermal equilibrium with each other.⁹

The magnitude of the observed line intensity is then given by

$$I = \left(\frac{CgA}{\lambda} \right) e^{-E/kT} \quad (1)$$

where g is the statistical weight of the upper state involved in the transition, A is the transition probability, λ is the wavelength, E is the excitation energy of the upper state, T is the electron temperature, and C is a constant which includes a geometric collection factor.

Taking the log and rearranging, Eq. (1) becomes

$$\ln \left(\frac{\lambda I}{gA} \right) = \ln(C) - \frac{E}{kT} \quad (2)$$

Fig. 1 is a plot of the experimental values for the LHS of Eq. (2) as a function of the excitation energies of the observed lines. With the

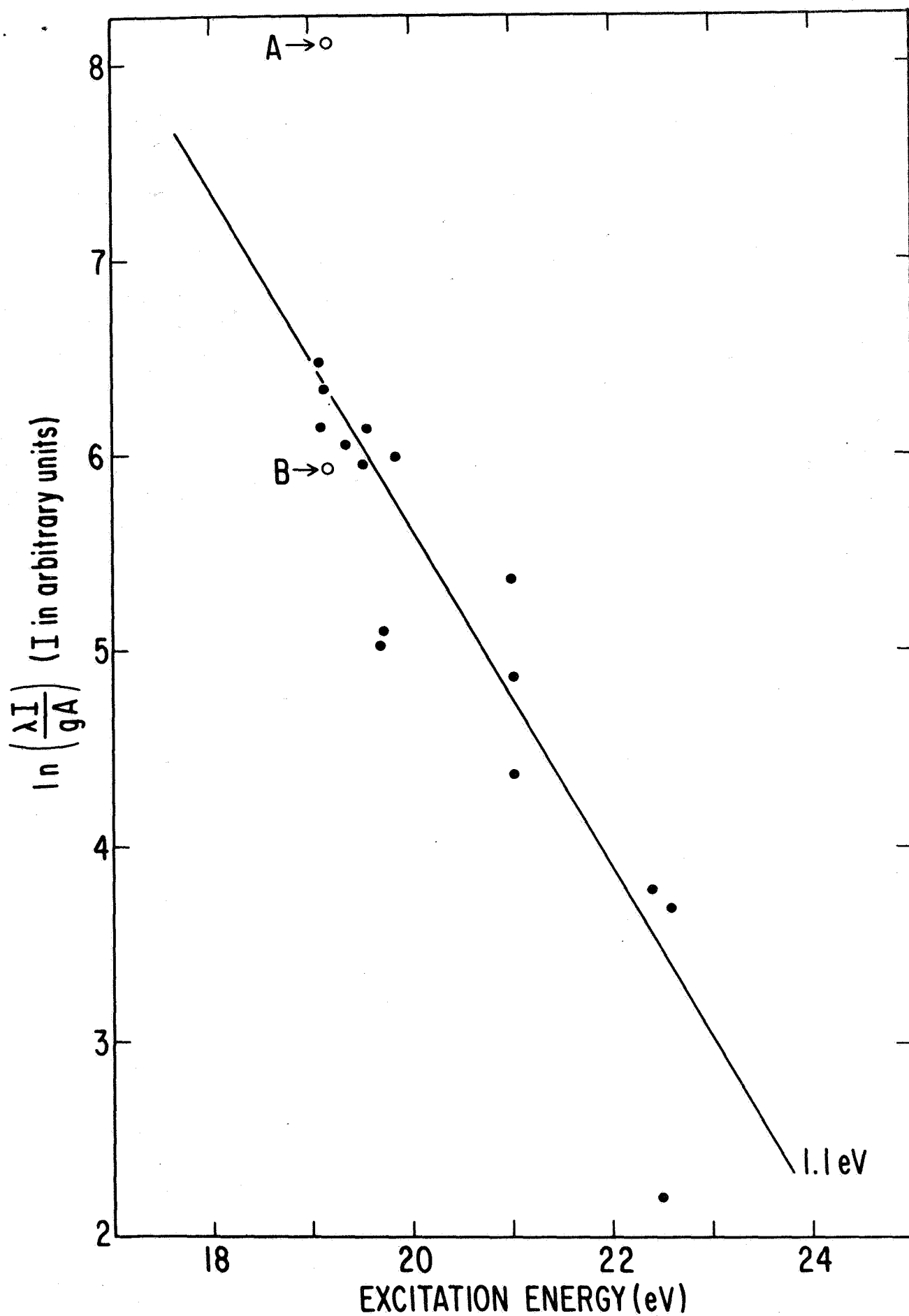


Fig. 1. Plot of $\ln(\lambda I/gA)$ vs. excitation energy for spectral lines of Argon II.

exception of point A, the data seems to fit a straight line. The slope of the least square fit corresponds to an electron temperature of 1.1 ± 0.2 eV.

The above procedure was repeated for several points in the radial interval from $R = 2.0$ to 4.0 cm with the same result. Fig. 2 shows the azimuthal variation of T_e at a radius of $R = 3.0$ cm. The radial component of the arc current density is included as a reference. The current spoke is moving from right to left in this presentation.

The observed intensity of the 4847.9 \AA line, labeled A in Fig. 1, is almost an order of magnitude higher than the expected value. The discrepancy was found to be the result of an incorrect experimentally determined transition probability reported in the literature.¹⁰ Point B is the data point plotted again, but this time using the theoretical value for the transition probability.¹¹⁻¹² The data in Fig. 1 therefore confirms the validity of the theoretical calculation.

2. Azimuthal Plasma Velocity

The measurement of the azimuthal plasma velocity was necessary to determine whether the current spoke was an azimuthally propagating ionization wave or an actual plasma rotation.

The plasma velocity can be measured indirectly by utilizing the generalized Ohm's law.

$$\vec{\eta J} = \vec{E} + \vec{v} \times \vec{B} - \frac{1}{ne} [\vec{J} \times \vec{B} - \vec{\nabla} p_e] \quad (3)$$

The electron pressure gradient term is negligible in both the radial and axial directions, but not quite negligible in the azimuthal direction.

The components of Ohm's law are then

$$\eta J_r = E_r - v_\theta B_z \quad (4)$$

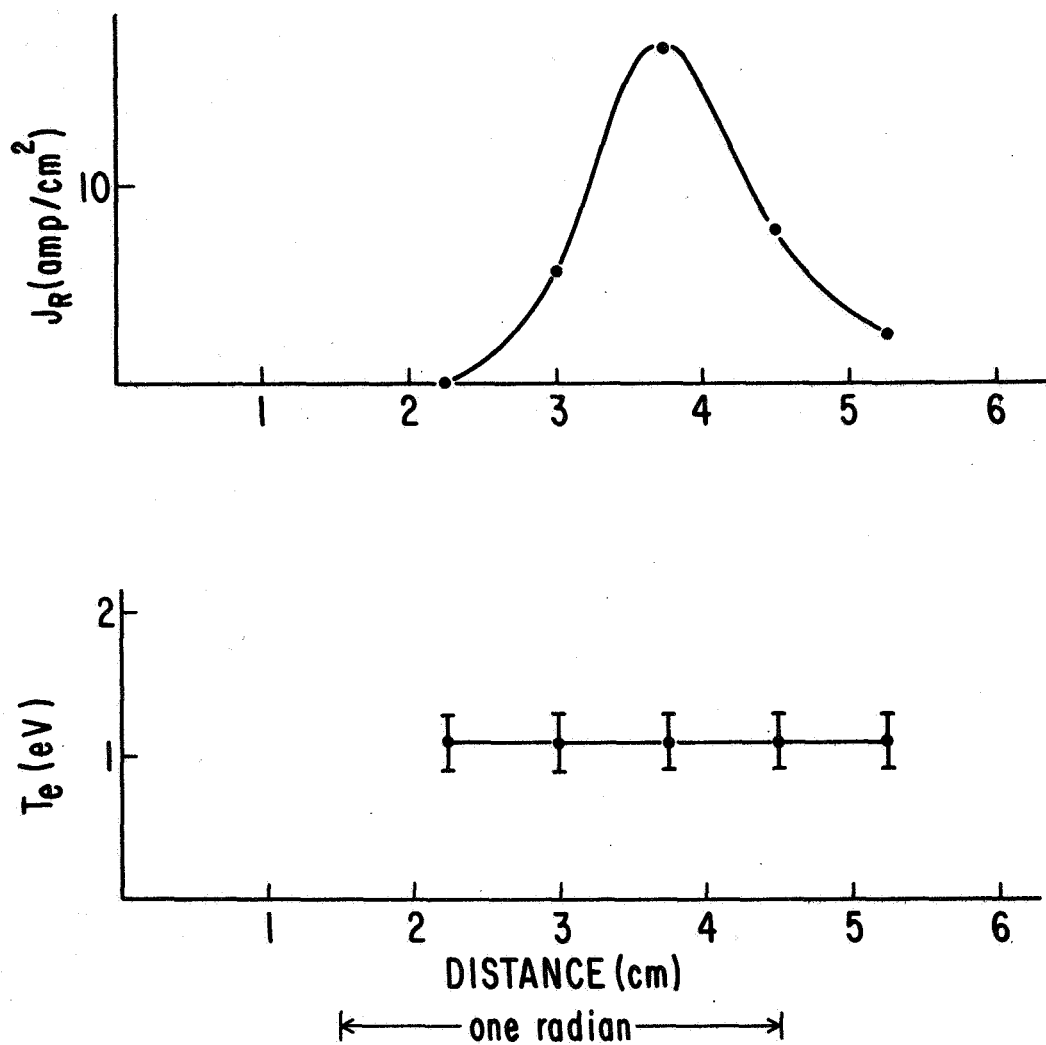


Fig. 2. Radial arc current density and electron temperature vs. azimuthal distance at a radius of 3.0 cm.

$$0 = E_{\theta} + V_R B_z + V_z B_R - \frac{1}{ne} [J_R B_z + J_z B_R - \nabla_{\theta} R] \quad (5)$$

$$\eta J_z = E_z - V_{\theta} B_R \quad (6)$$

where terms containing J_{θ} and B_{θ} have been neglected. These quantities are both small in the region of interest.

The positive directions for the quantities in Eqs. (4), (5) and (6) are shown in Fig. 3.

Negatively biased probes indicate the existence of a region of substantial plasma density just in front of the moving current spoke. In this region $J_r = J_z = 0$ and Eqs. (4) and (6) reduce to

$$V_{\theta} = \frac{E_R}{B_z} \quad (7)$$

and

$$V_{\theta} = \frac{E_z}{B_R} \quad (8)$$

All of the field components on the RHS of Eqs. (7) and (8) have been measured directly and the calculated values of the azimuthal plasma velocity are equal to the velocity of the current spoke, i.e.

$$V_{\theta} = \omega R = 7.5 \times 10^5 \text{ cm/sec}$$

at a radius of $R = 3.0$ cm. This agreement is shown in Figs. 8 and 9. The first four triangles in each plot are calculated from Eqs. (7) and (8) respectively, assuming that $V_{\theta} = \omega R$.

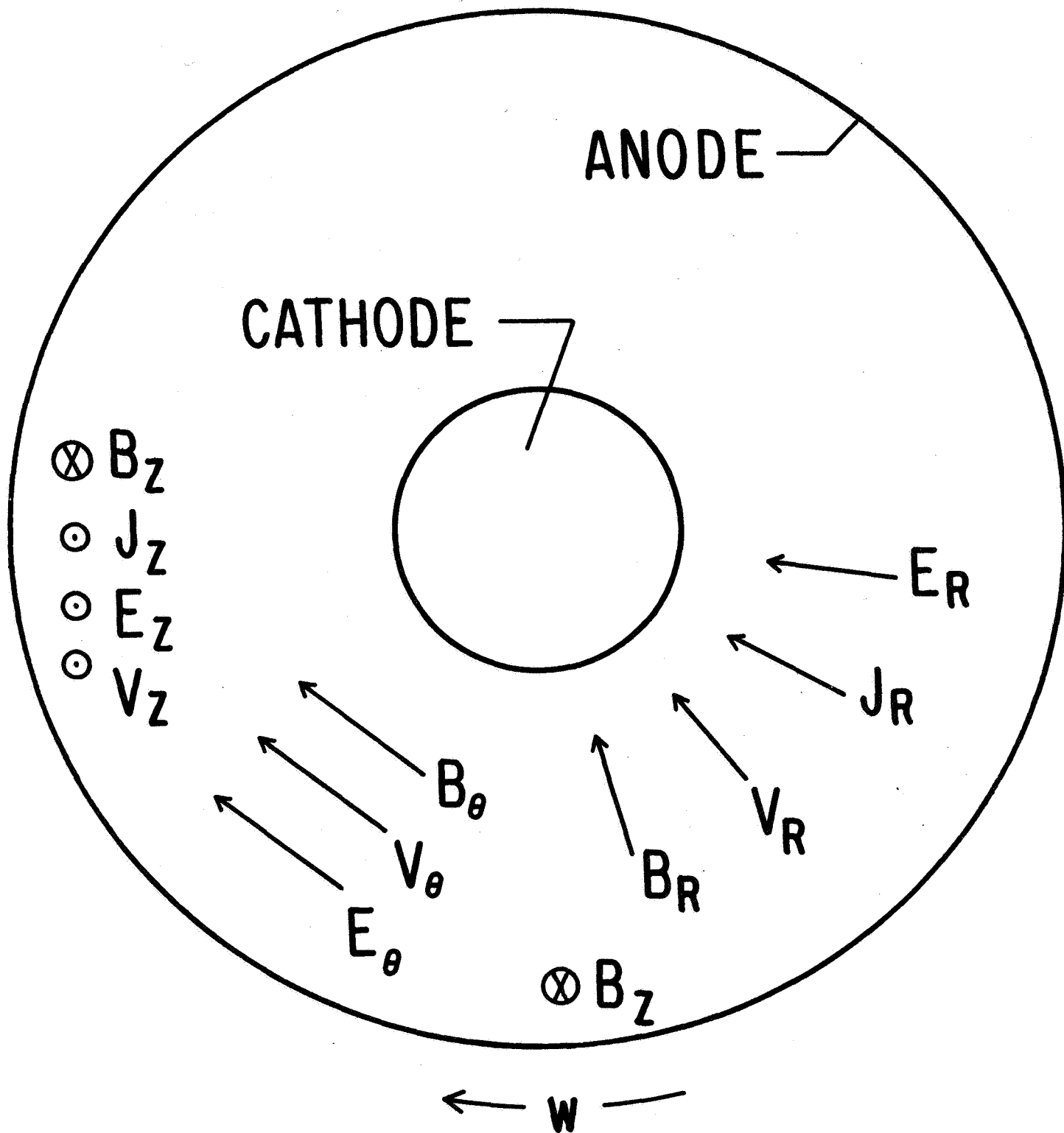


Fig. 3. Positive directions assumed for components of E , B , v , and J .

3. Plasma Flux Measurements in the Spoke

Negatively biased Langmuir probes have been used to measure plasma fluxes and velocities. The theory of Langmuir probes is very complicated, particularly in a magnetic field. However, because of the fortunate set of circumstances discussed below, the analysis is greatly simplified in the MPD arc.

- a) The ion gyro radius is very large compared to the probe dimensions. For strong negative bias, only ions are collected and the effects of the magnetic field can be neglected.
- b) The Debye length is about 5×10^{-4} cm. The sheath dimensions are therefore very small compared to the probe dimensions and orbital effects can be neglected.
- c) The ion velocities relative to the probe are large compared to the "Bohm velocity"

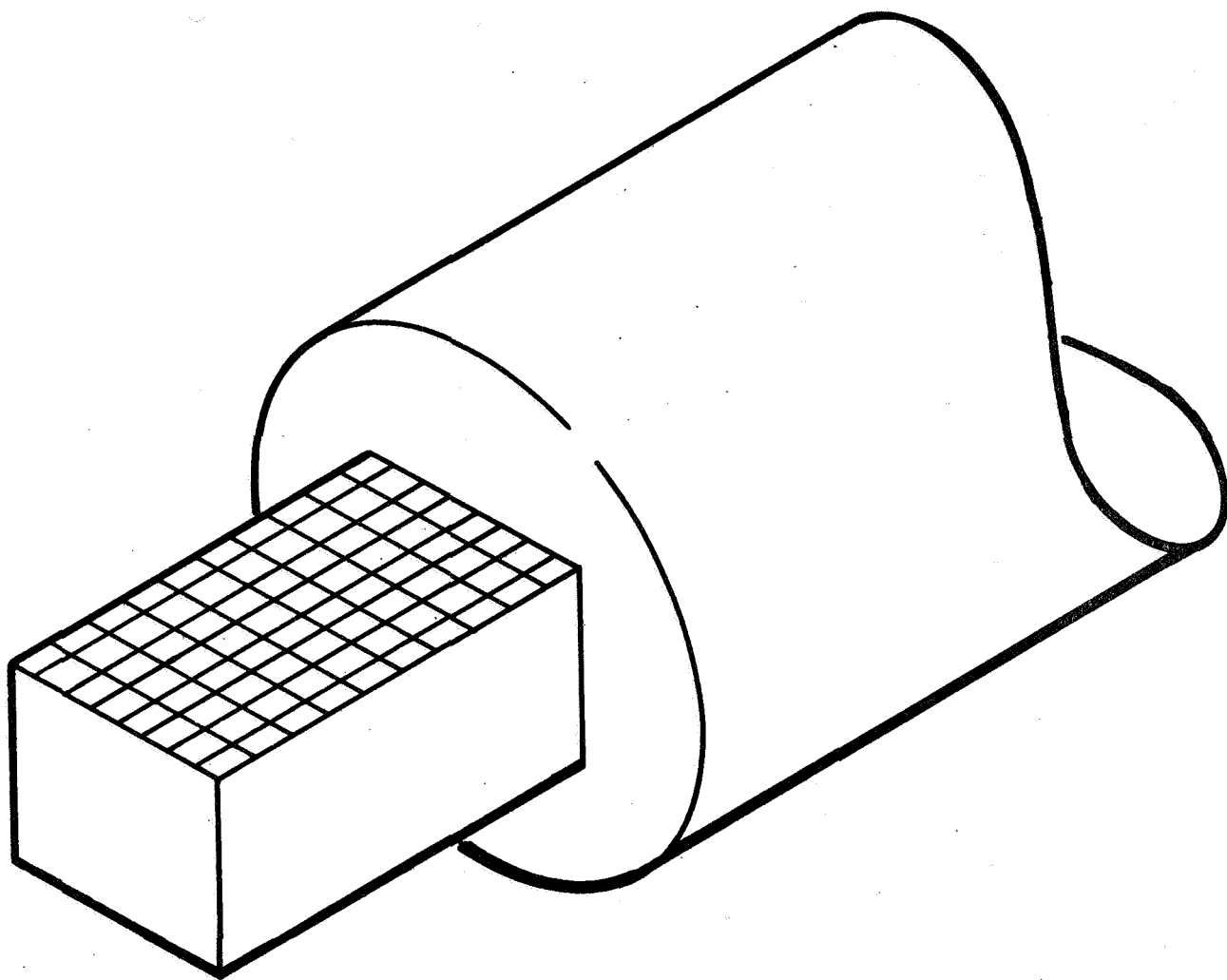
$$V_B = \left(\frac{kT_e}{m_i} \right)^{1/2}$$

The Bohm criterion for the existence of a stable sheath is satisfied and the simple theory of Langmuir is valid.

- d) The ion-ion mean free path is large compared to the probe dimensions. The perturbation produced by the probe can therefore be neglected.

The double plane Langmuir probe is shown schematically in Fig. 4. It consists of two plane electrodes located on opposite sides of the probe. Both electrodes are biased strongly negative so that each collects all of the ions moving towards it. The current collected by the front electrode is j_F which is given by

$$j_F = e \int_0^{\infty} v_x f(v_x) dv_x$$



DOUBLE PLANE LANGMUIR PROBE

Fig. 4. Sketch of double plane Langmuir probe used in plasma flux measurements.

$$j_F = e \int_{-\infty}^{\infty} v_x f(v_x) dv_x - \int_{-\infty}^0 v_x f(v_x) dv_x$$

$$= ne \bar{v}_x + j_R$$

where j_R is the ion saturation current density collected by the rear electrode. The plasma flux is therefore given by

$$n \bar{v}_x = \frac{1}{e} (j_F - j_R) \quad (9)$$

where \bar{v}_x is the average plasma velocity component normal to the surfaces of the electrodes.

Fig. 5 shows the radial dependence of the currents to the front and rear electrodes of a probe positioned at the mouth of the anode and oriented in the azimuthal direction. The azimuthal plasma flux, which is given by the difference between the two signals, is approximately proportional to the radius. This implies that the plasma density is nearly independent of radius since

$$n \bar{v}_\theta = n \omega R$$

The magnitude of the peak density can be obtained from the slope of the data in Fig. 5.

$$n = \frac{1}{e \omega} \frac{d}{dR} (j_F - j_R)$$

$$= 10^{14} \text{ cm}^{-3}$$

There exists independent evidence for the lack of a radial dependence in the density. The intensities of AII spectral lines did not vary with radius. Since the electron temperature was found to be independent of

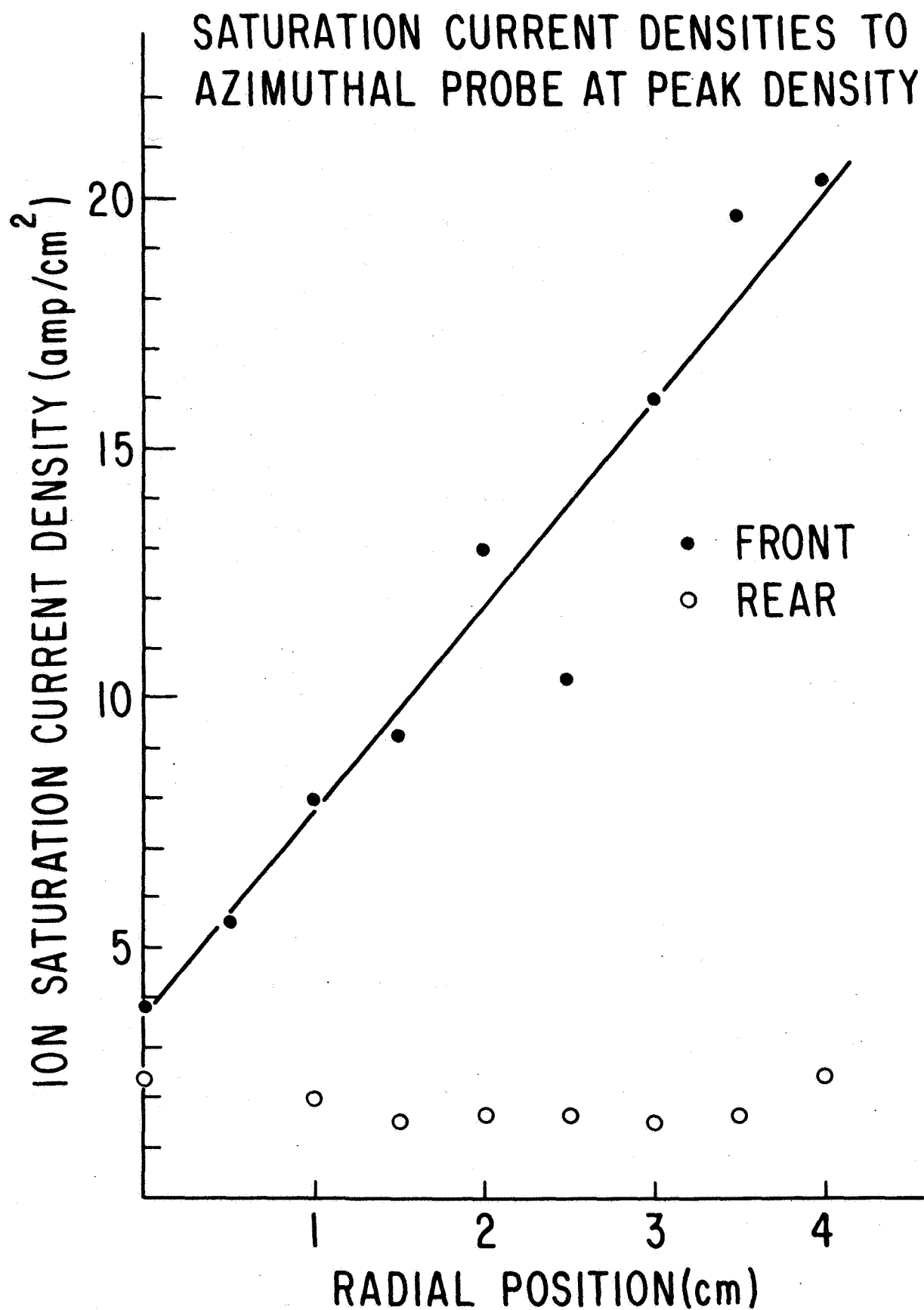


Fig. 5. Radial dependence of ion saturation currents to front and rear electrodes of double plane Langmuir probe.

radius, the ion density must also be constant.

Since the azimuthal plasma velocity is equal to that of the current spoke, the density profile in the azimuthal direction was obtained directly from the azimuthal plasma flux.

$$n_i = \frac{1}{e\omega R} (j_F - j_R)_\theta \quad (10)$$

A plot of ion density vs. azimuthal distance is shown in Fig. 6 for a radius of 3.0 cm. at the mouth of the anode. Again the radial component of the arc current density is included as a reference.

With the ion density profile determined, the probe was oriented in the radial and axial directions in order to measure the profile of these velocity components. They are given by

$$\bar{V}_R = \frac{1}{ne} (j_F - j_R)_R \quad (11)$$

$$\bar{V}_z = \frac{1}{ne} (j_F - j_R)_z \quad (12)$$

The results are shown in Fig. 7 for a radius of 3.0 cm.

The radial velocity profile shows the existence of counter-streaming plasma flows. The plasma in front of the current spoke is moving outward, probably because of the centrifugal force. In the current spoke, however, the ions are moving inward and therefore carry a portion of the arc current.

The portion of the radial arc current density carried by ions is

$$J_{ion} = ne \bar{V}_R \quad (13)$$

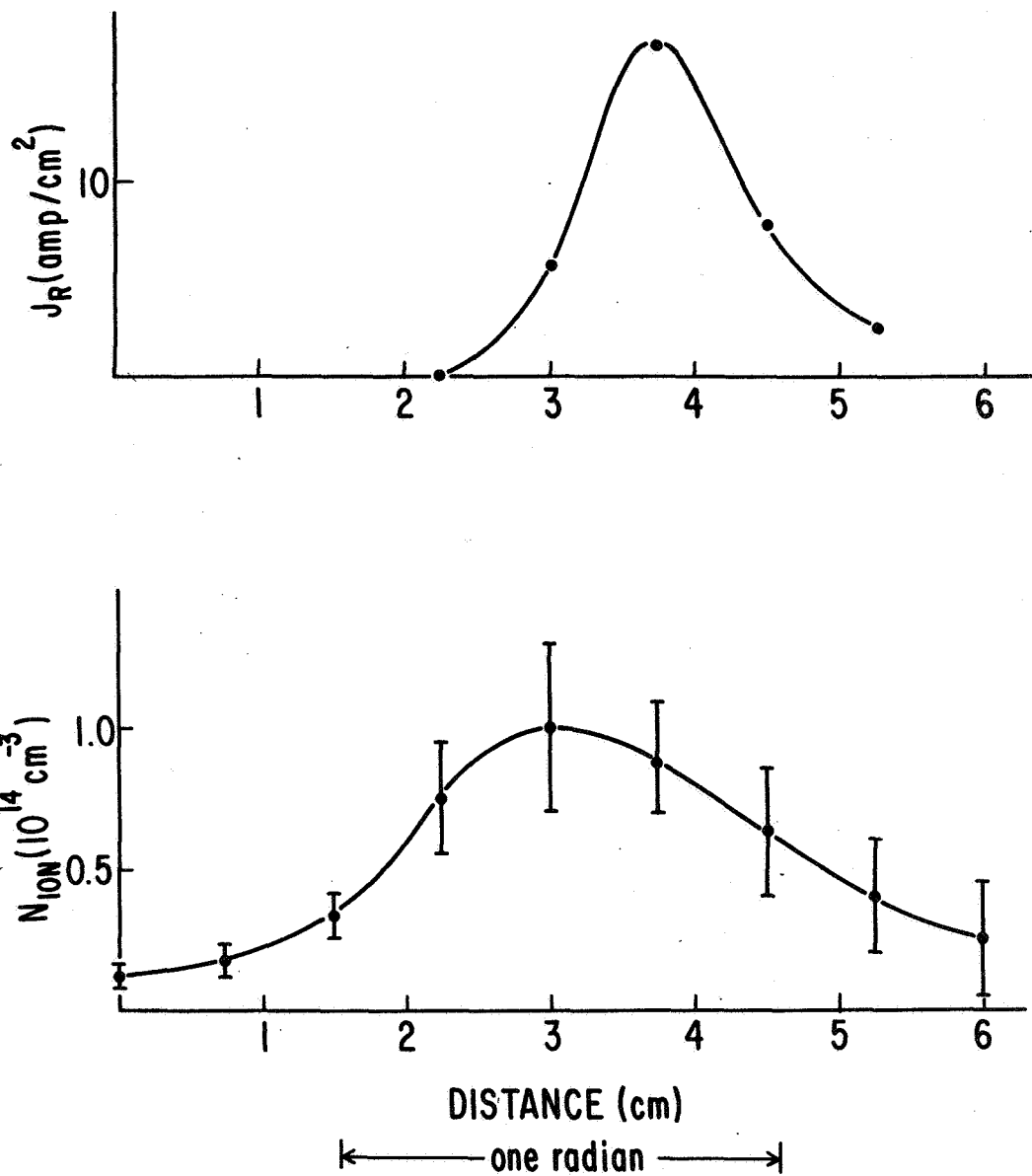


Fig. 6. Radial arc current density and ion density vs. azimuthal distance at a radius of 3.0 cm.

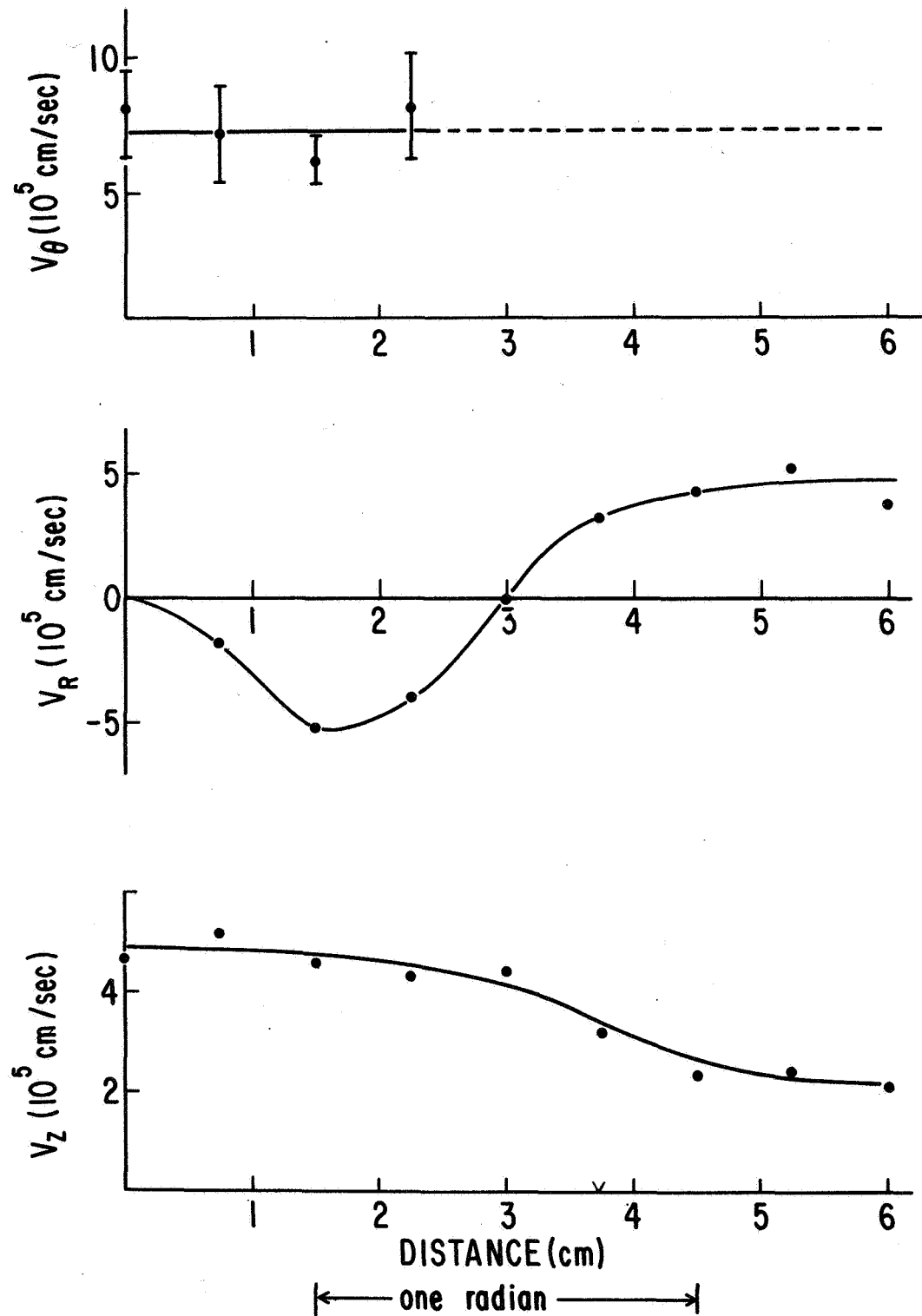


Fig. 7. Plasma velocity components vs. azimuthal distance at a radius of 3.0 cm.

while that carried by the electrons is

$$J_{el} = ne \left(\frac{E_{\theta}^*}{B_z} \right) - ne \bar{v}_e \quad (14)$$

where E_{θ}^* is the azimuthal component of the electric field in the plasma rest frame. The values of the ion and electron current densities calculated from Eqs. (13) and (14) on the axis of the current spoke at $R = 3.0$ cm are

$$J_{ion} \simeq 5 \text{ amp/cm}^2$$

$$J_{el} \simeq 13 \text{ amp/cm}^2$$

thus roughly 30% of the radial arc current is carried by ions and 70% by electrons.

4. Plasma Resistivity

The measurements described in the preceding sections have determined all of the quantities in the component equations of the generalized Ohm's law, Eqs. (4), (5), (6).

It is now possible to compare direct measurements with values deduced from other measured quantities via Ohm's law. Because the greatest data scatter occurred in the electric field measurements, the electric field components are used for the comparison. Rewriting Eqs. (4), (5) and (6)

$$E_R = \eta J_R + V_{\theta} B_z \quad (15)$$

$$E_{\theta} = \frac{1}{ne} [J_R B_z - J_z B_R] - V_R B_z - V_z B_R - \frac{1}{ne} \nabla_{\theta} p_e \quad (16)$$

$$E_z = \eta J_z + V_{\theta} B_R \quad (17)$$

Figs. 8, 9 and 10 show the measured values of the electric field components as black circles with error bars and the values calculated from Eqs. (15), (16) and (17) as triangles. The resistivity used in Eqs. (15) and (17) had

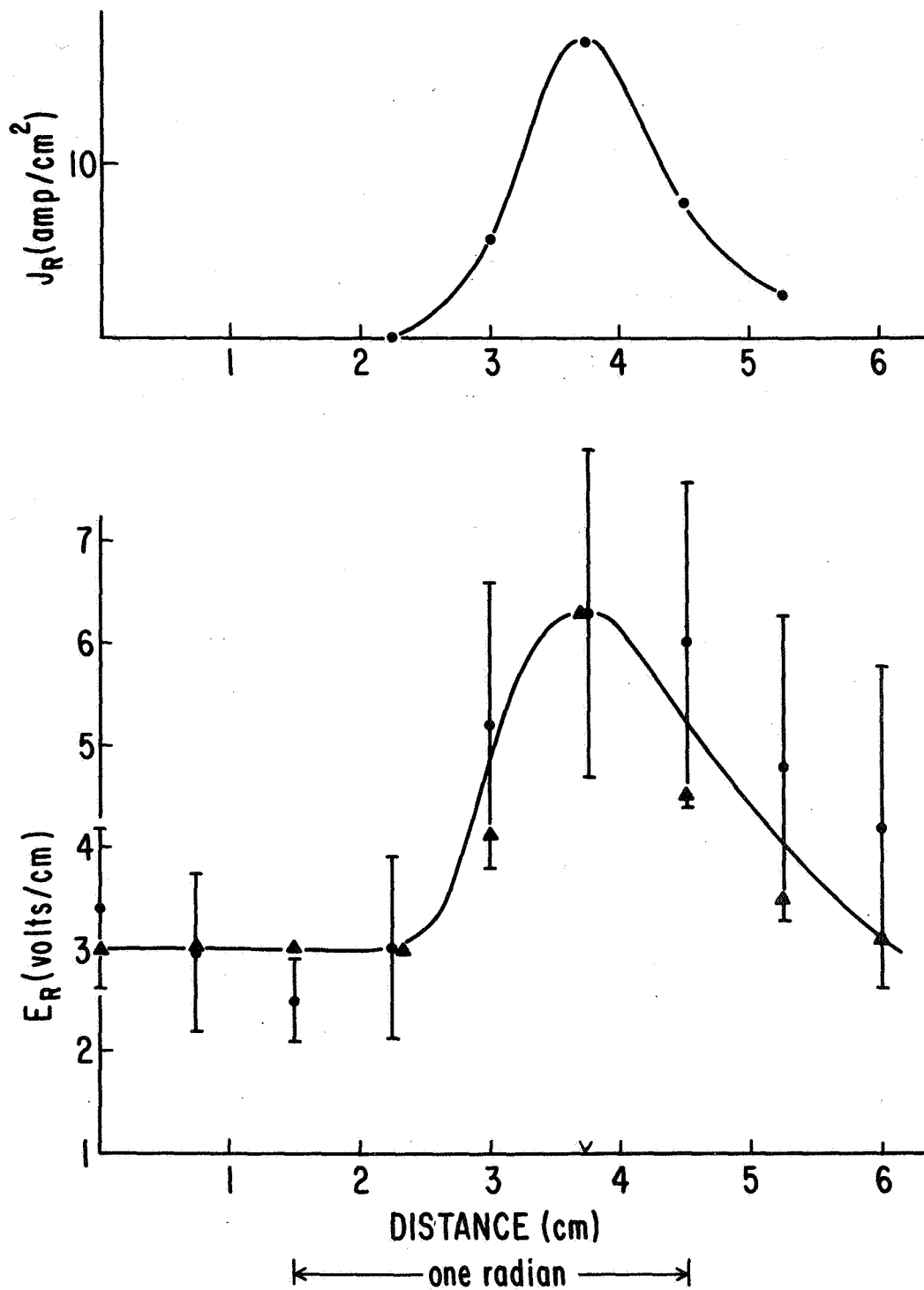


Fig. 8. Radial electric field vs. azimuthal distance at a radius of 3.0 cm. Directly measured values are shown as circles, while calculated values are plotted as triangles.

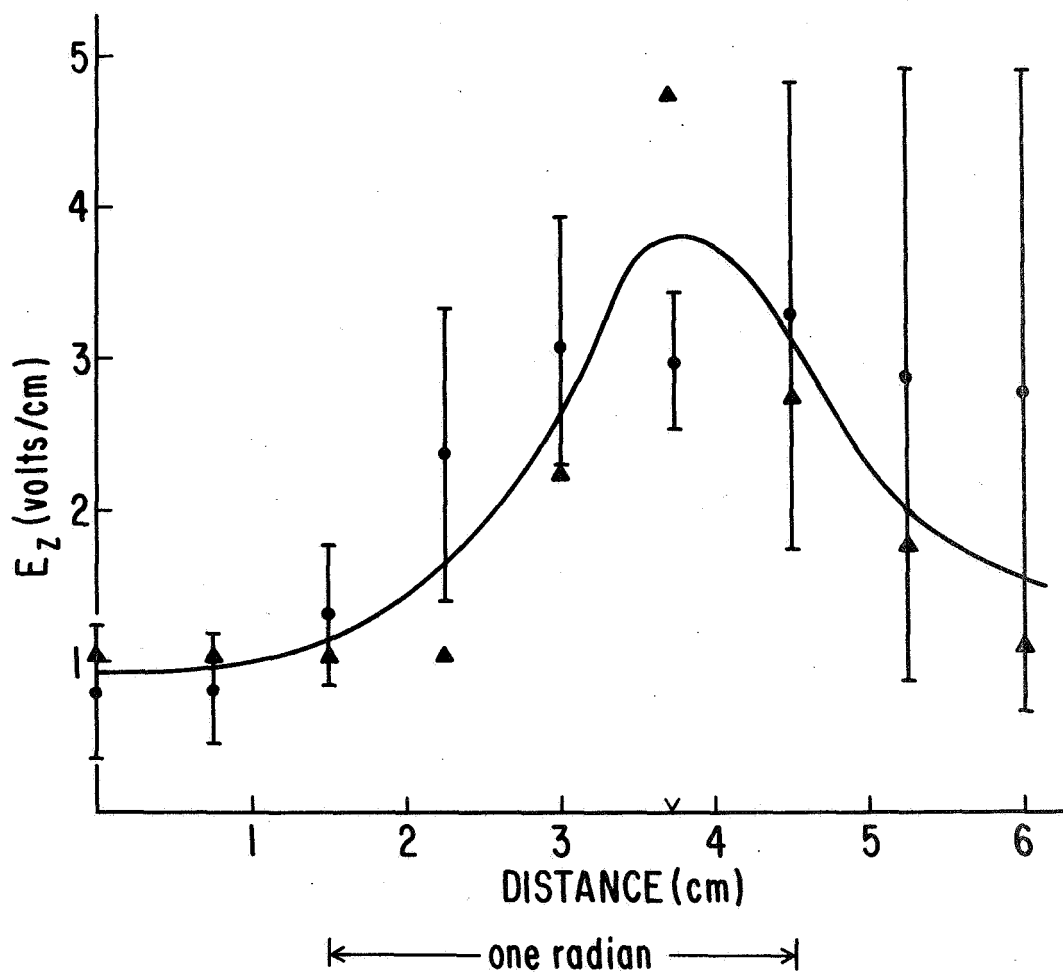


Fig. 9. Axial electric field vs. azimuthal distance at a radius of 3.0 cm. Directly measured values are shown as circles, while calculated values are plotted as triangles.

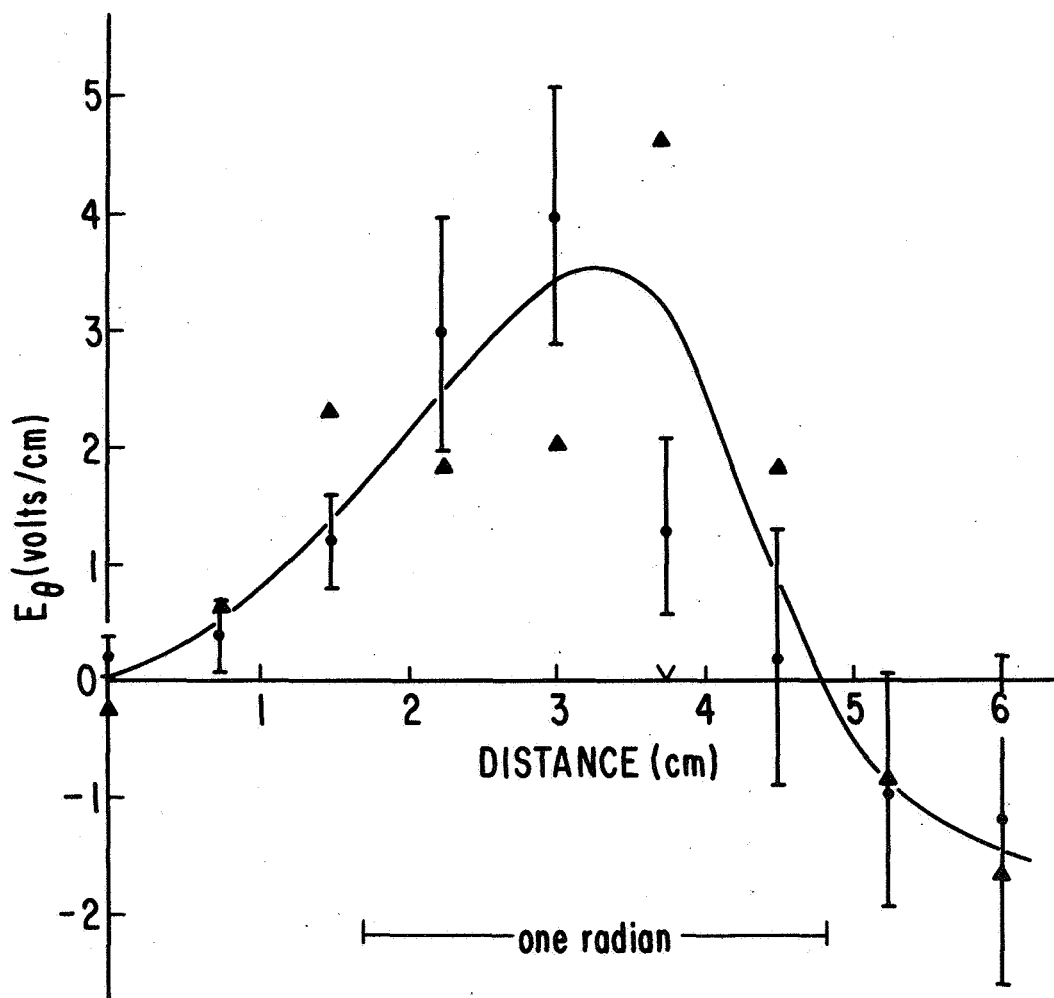


Fig. 10. Azimuthal electric field vs. azimuthal distance at a radius of 3.0 cm. Directly measured values are shown as circles, while calculated values are plotted as triangles.

to be approximately four times as large as the value calculated from Spitzer's formula. Circulated values of E_r and E_z using Spitzer's value were well outside of the error bars of the measurements. The observed resistivity is therefore

$$\eta_{obs} = (4.0 \pm 1.5) \eta_{Spitzer} \quad (18)$$

The azimuthal component of Ohm's law does not include the resistivity. The azimuthal electric field therefore provides a check for internal consistency of the input data for the right hand side of Eq. (16).

The rather complicated deduction process described in Sections III-2 through III-4 are outlined in the flow diagram shown in Fig. 11. The boxes enclose directly measured quantities, while inferred quantities are enclosed in circles.

5. Ion Temperature

An order of magnitude estimate of the ion temperature was obtained by rotating the double plane Langmuir probe in the R- θ plane until the electrode surfaces were parallel to the net plasma streaming velocity. In this orientation the ion saturation currents to the two electrodes are identical and due entirely to thermal motions. The magnitude of the ion saturation current is given by one of the following expressions depending on whether the electron temperature is greater or less than that of the ions.¹³

$$j_{sat} \approx 0.5 n e \left(\frac{k T_e}{m_i} \right)^{1/2} \quad T_i < T_e$$

$$j_{sat} \approx \left(\frac{1}{2\pi} \right)^{1/2} n e \left(\frac{k T_i}{m_i} \right)^{1/2} \quad T_i > T_e$$

Substituting the measured values of j_{sat} and n

$$kT \approx 11 \text{ eV}$$

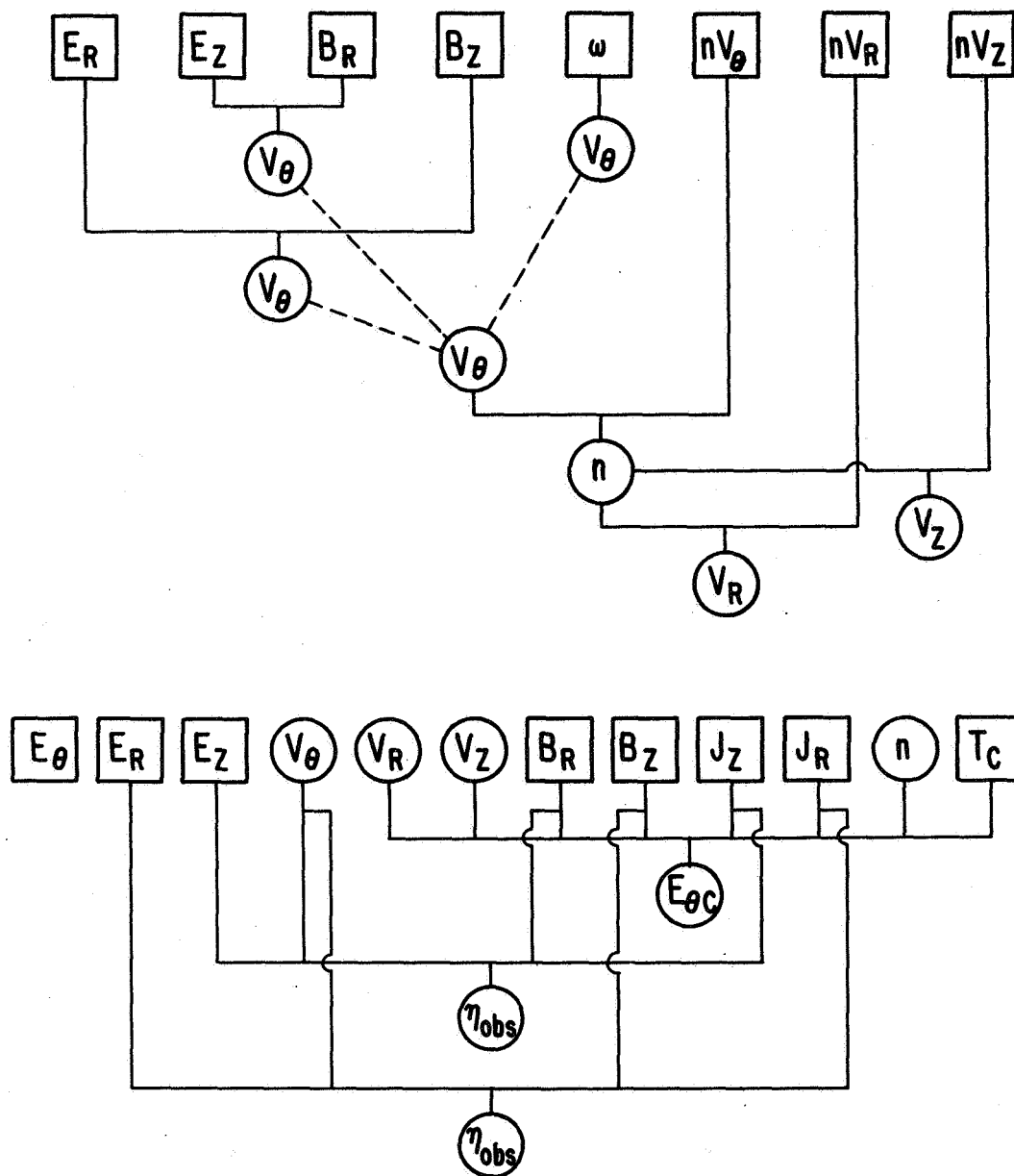


Fig. 11. Flow diagram showing the combinations of observed quantities used to deduce plasma properties. The boxes enclose directly measured quantities, while inferred quantities are enclosed in circles.

Since kT_e has been measured spectroscopically to be 1.1 eV, it is clearly the ion temperature that is of the order of 11 eV.

The same observations were made at radii of 3.25 cm and 2.75 cm with the results shown in Table I.

TABLE I

R (cm)	kT_i (eV)	$E_o = \frac{1}{2} m v^2 R^2$ (eV)
3.25	12	14
3.0	11	12
2.75	9	10

E_o is the stagnation energy or the kinetic energy of the incoming neutral atoms when viewed from the rest frame of the spoke. The uncertainty in the measured ion temperatures is about $\pm 50\%$, therefore the apparent equality between the ion temperature and the stagnation energy may not be exact, but they are of the same order of magnitude.

The ion-ion mean free path at an energy of 10 eV is approximately 2.5 cm, which is nearly 30 times greater the probe dimensions. The 10 eV ion temperature and the corresponding ion-ion mean free path of 2.5 cm justify the statements made in III-3 (c) and (d).

The ion saturation current to the rear electrode of the azimuthally oriented probe seems to support the contention that the ion temperature is roughly equal to the stagnation energy. Assuming a Maxwellian velocity distribution for the ions, the ion saturation current density to the rear electrode is

$$j_r = ne \bar{c}_i F(\bar{v}/\bar{c}_i) \quad (19)$$

where V_s is the plasma streaming velocity and

$$\bar{c}_i = \left(\frac{2kT_i}{m_i} \right)^{1/2}$$

$$F(x) = (4\pi)^{-1/2} \exp(-x^2) - \frac{x}{2} [1 - \operatorname{erf}(x)]$$

The function $F(x)$ is a strongly varying function of x --a factor of two change in $x = \frac{V_s}{\bar{c}_i}$ produces two orders of magnitude change in $F(x)$. Fig. 5 shows the ion saturation current to the rear electrode to be at most a weak function of radius. The ratio (V_s/\bar{c}_i) must therefore be nearly constant. The value of j_R calculated from Eq. (19), assuming that the ion temperature equals the stagnation energy, is approximately $\frac{1}{2}$ of the observed values given in Fig. 5. This agreement is not bad considering the range over which $F\left(\frac{V_s}{\bar{c}_i}\right)$ varies.

6. Energy Analysis in Exhaust

An energy analysis of the plasma in the exhaust was made using the electrostatic analyzer shown schematically in Fig. 12. It consists of an expansion chamber to lower the plasma density and two negatively biased grids to separate the electrons from the ions and to suppress secondary emission. A collector with variable bias collected all ions having an energy greater than the collector potential relative to the plasma space potential.

The analyzer output consists of a steady d.c. component plus an a.c. component which oscillates with a frequency equal to the rotation frequency of the arc. The fractional modulation of the output increases with increasing collector bias potential and attains a value of 100% at a bias potential of about 50 volts. Fig. 13 is a plot of the analyzer output as a function

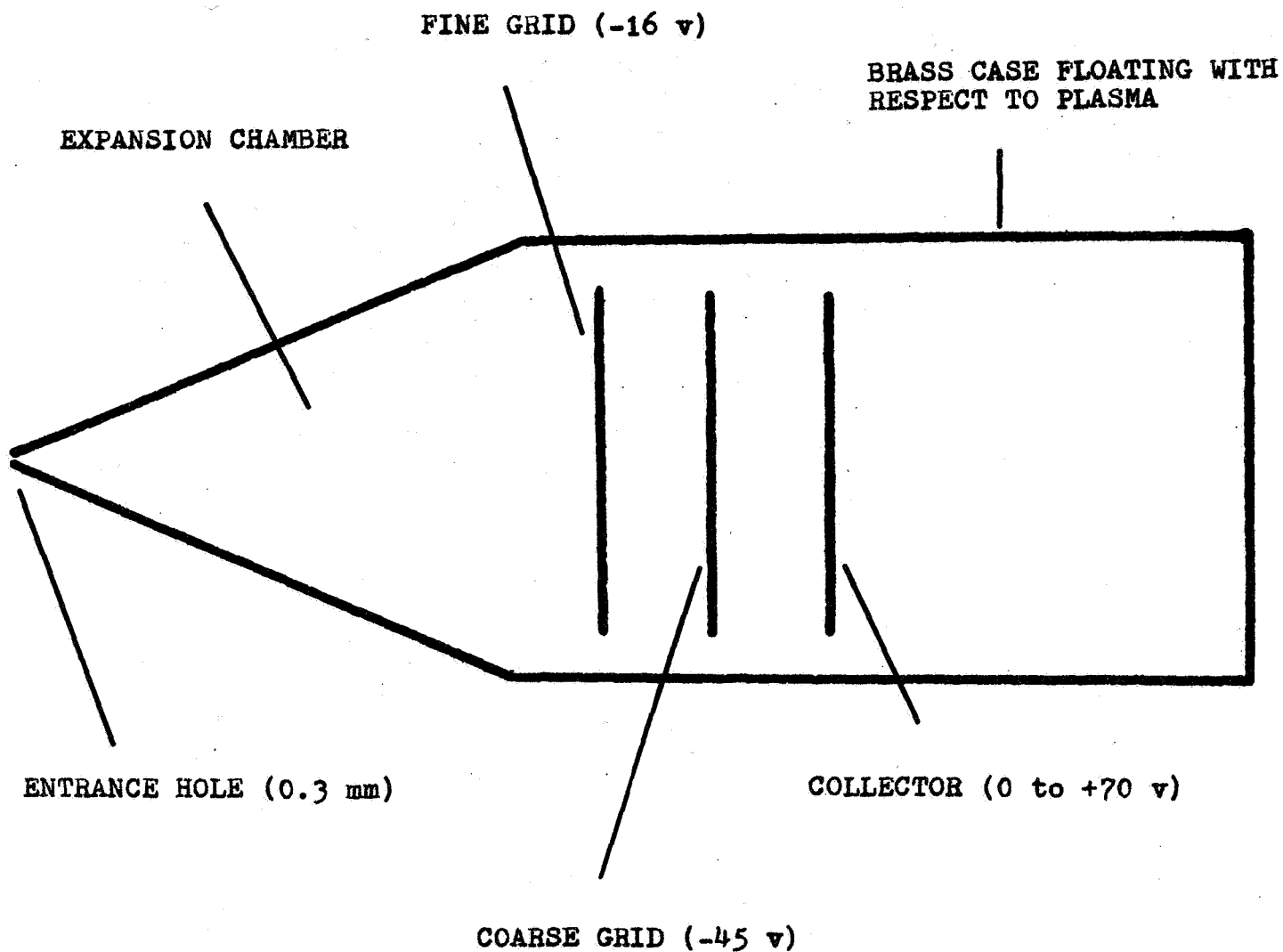


Fig. 12. Schematic drawing of energy analyzer. All voltages are measured with respect to the brass case.

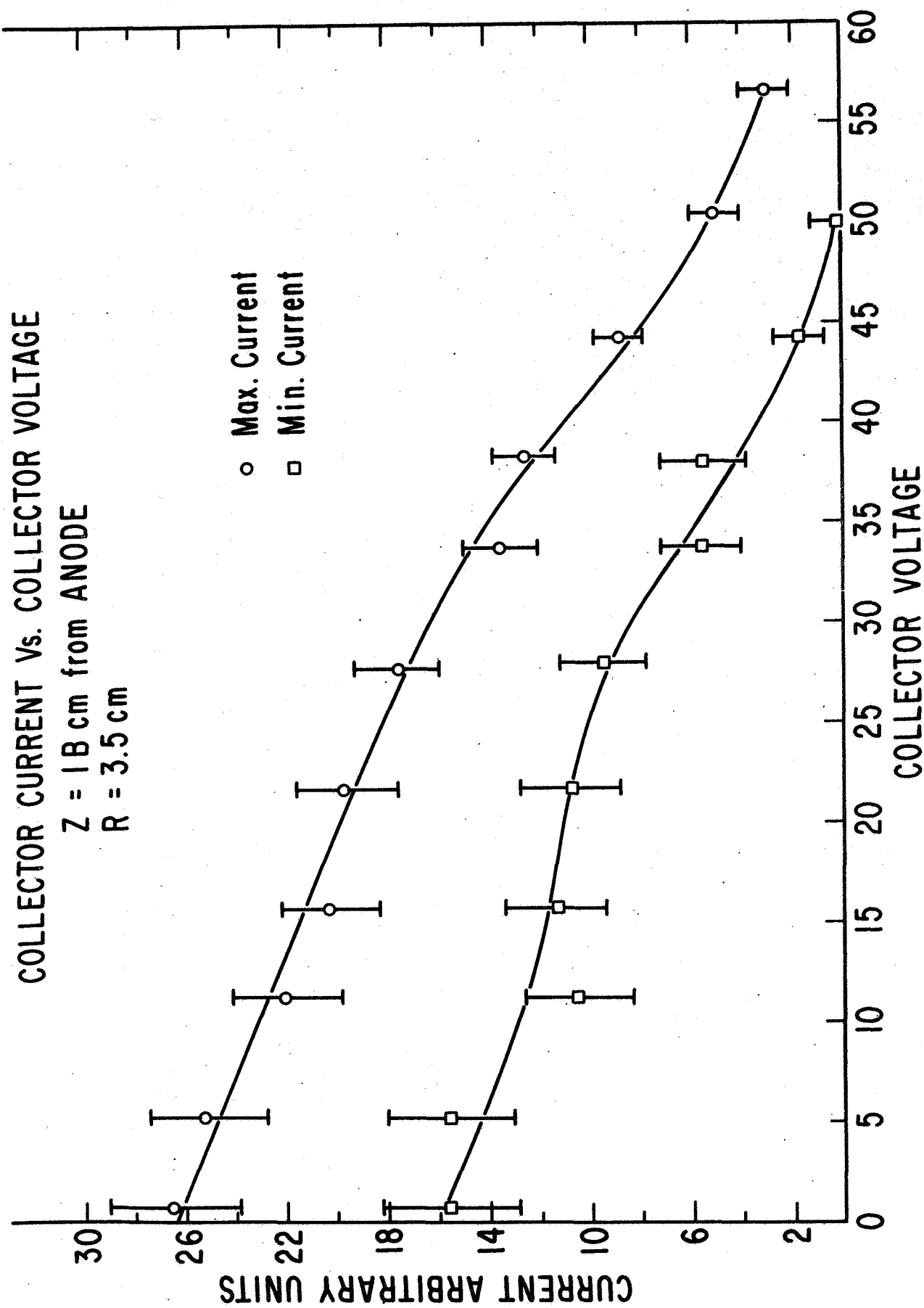


Fig. 13. Output current of energy analyzer as a function of collector voltage. Analyzer positioned 18 cm downstream of anode at a radius of 3.5 cm with its axis parallel to that of the accelerator.

of collector bias potential for a run made 18 cm downstream of the anode at a radius of $R = 3.5$ cm. The ion distribution function is given by the slope of the output data from the analyzer, i.e.

$$f(v_i) \propto \left. \frac{dI_c}{dV_c} \right|_{V_c = \frac{mv_i^2}{2e}} \quad (20)$$

where I_c is the analyzer collector current and V_c is the analyzer bias voltage. The data of Fig. 13 indicates a rather broad distribution of ion energies up to cutoff in the 50 to 60 ev range, with some peaking in the distribution at energies between 35 and 50 ev.

7. Plasma Flux Measurements in the Exhaust

The double Langmuir probe described in Section III-3 was used to measure the plasma flux in the exhaust region. The projections of the peak observed flux $n\vec{v}$ on the R- θ and R-Z planes are shown in Figs. 14 and 15 for probes at positions 2 cm and 4 cm downstream of the anode. The direction of the magnetic field vectors are also included in the figures for reference. It is evident from the data that the plasma in the exhaust is moving radially across the magnetic field lines. The magnetic field is therefore not functioning efficiently as a magnetic nozzle.

The axial plasma flux is observed to originate in the plasma spoke. Since the spoke has a limited azimuthal extent, the time averaged axial flux at $R = 0$ is larger than that at any other radial position. The time averaged thrust is therefore also greatest near the axis of the arc.

IV. Conclusions

1. The arc has the form of a rotating spoke. The electron temperature is quite uniform throughout the plasma spoke, and the ion density is nearly independent of radius. The ion density outside the plasma spoke is at least an order of magnitude less than that in the spoke.

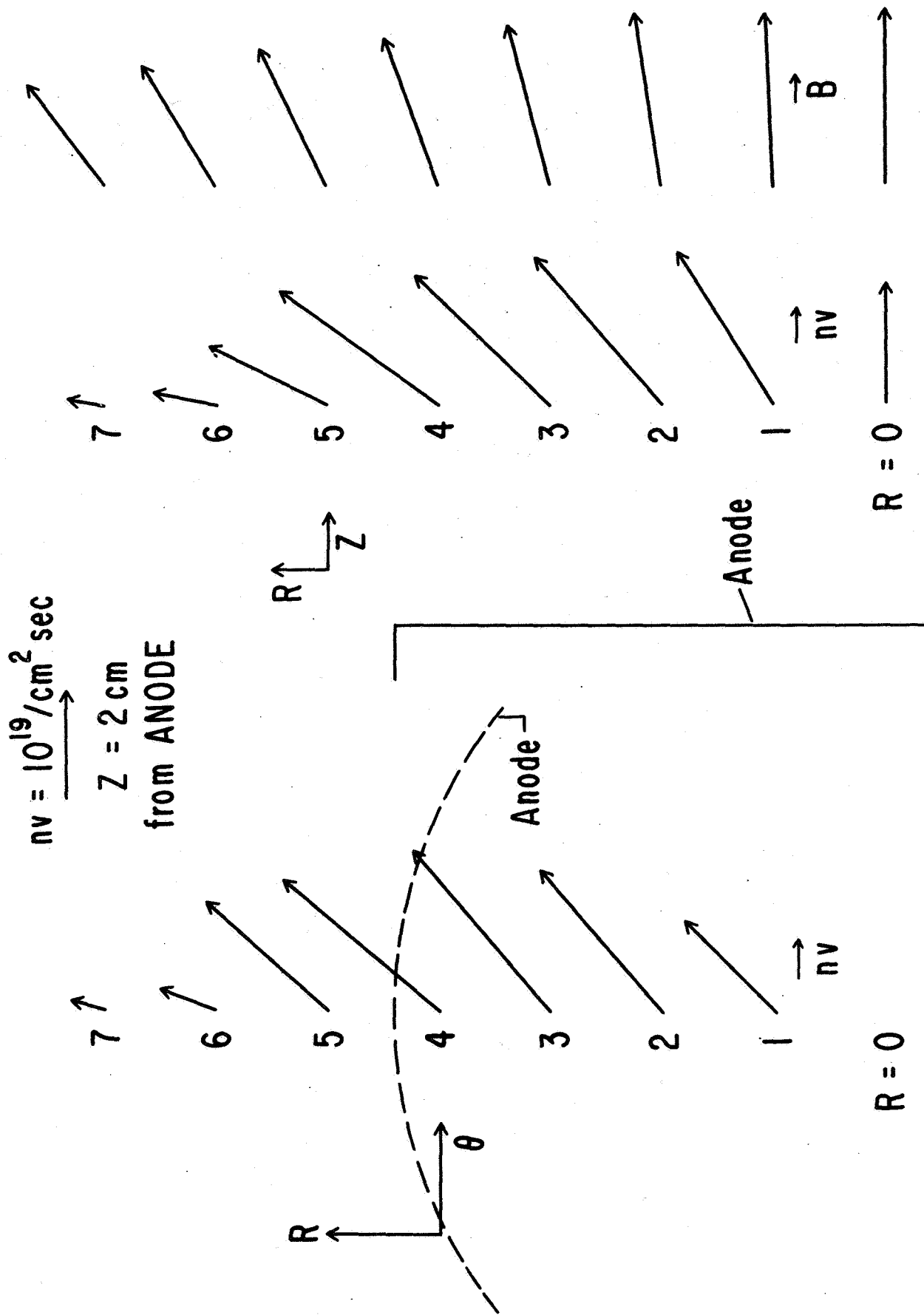


Fig. 14. Projections of the peak plasma flux and magnetic field on the R- θ and R-Z planes for probe positioned 2 cm downstream of the anode.

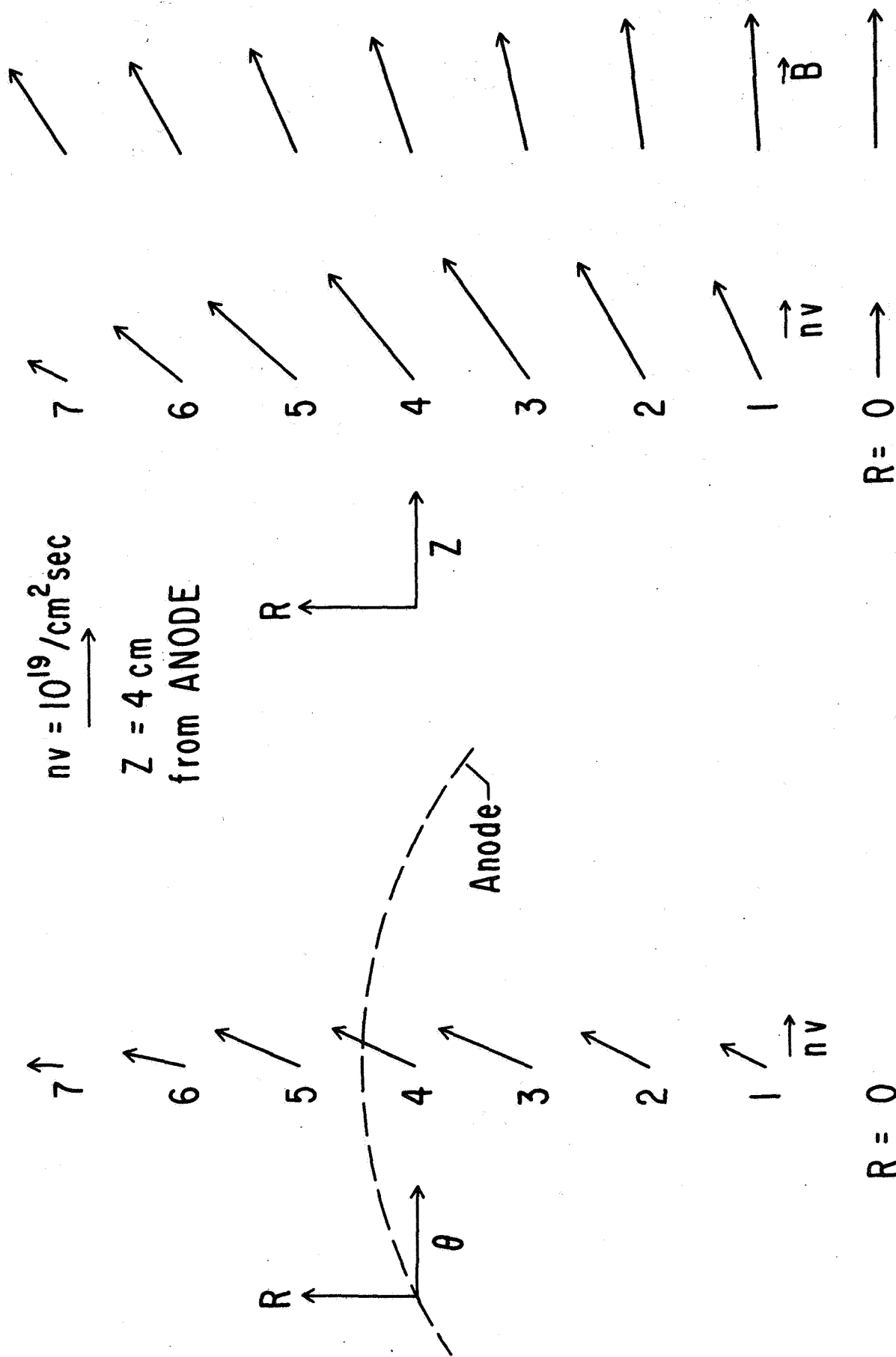


Fig. 15. Projections of the peak plasma flux and magnetic field on the R- θ and R-Z planes for probe positioned 4 cm downstream of the anode.

2. The azimuthal extent of the plasma is greater than that of the current spoke, with the result that a plasma region exists ahead of the current spoke. This advanced plasma is moving azimuthally with the spoke velocity and appears to be spun out radially by the centrifugal force.

3. The plasma within the current spoke is counterstreaming radially inward indicating the presence of an inward force greater than the centrifugal force. The ion pressure gradient seems to be the most likely candidate. In accordance with the data listed in Table I

$$kT_i = \beta E_0$$

where β is a factor of order one and E_0 is the stagnation energy. Thus

$$kT_i = \frac{1}{2} \beta m \omega^2 R^2 \quad (21)$$

The radial component of the volume force due to the ion pressure gradient is

$$\begin{aligned} F_r &= -\nabla_r p_i \\ &= -\nabla_r (n k T_i) \end{aligned} \quad (22)$$

Since the density n has been observed to be independent of R , Eqs. (21) and (22) together give

$$\begin{aligned} F_r &= -\beta n m \omega^2 R \\ &= -\beta F_{\text{cent}} \end{aligned}$$

where F_{cent} is the centrifugal force per unit volume.

4. Although no azimuthal currents have been detected in the body of the arc, a current of about 50 amperes has been observed to flow azimuthally in the anode sheath. The resulting $J \times B$ force is directed inward and is of sufficient magnitude to overcome the net centrifugal force or equivalently to support the ion pressure gradient.

5. The observed resistivity is roughly four times as large as a value calculated from the Spitzer formula. Since Spitzer's assumptions of a Maxwellian electron distribution and large plasma parameter Λ seem to be satisfied, the anomalously high resistivity is suggestive of an enhanced electron scattering by microinstabilities or small scale plasma turbulence.

6. The ions seem to carry one-third of the radial arc current with the electrons carrying the remainder..

7. The average axially directed ion energy is far in excess of 3 ev per ion. Therefore, the acceleration of the plasma does not appear to be produced by a magnetic nozzle, i.e., by acceleration in the axial magnetic field gradient, since the electrons have only about 1 ev energy, and in the absence of ion coupling to the field, nozzle acceleration to about the electron energy is all that can be achieved.

We find, however, that direct $\mathbf{J} \times \mathbf{B}$ acceleration by the self-field of the arc is approximately adequate to produce the observed momentum flux, and hence, our conclusion, as opposed to our previous position, is that this device is not simply an arc heater, but acts as a direct MHD accelerator.

References

1. A. C. Ducati, G. M. Giannini and E. Muehlberger, AIAA J. 2, 1452 (1964).
2. R. M. Patrick and A. M. Schneiderman, AIAA J. 4, 283 (1966).
3. G. L. Cann, AIAA Bull. 1, 380 (1964).
4. W. Grossman, R. V. Hess and H. A. Hassan, AIAA J. 3, 1034 (1965).
5. S. Bennett, G. Enos, R. R. John and A. Tuchman, AIAA Bull. 2, 297 (1965).
6. R. Lovberg, First Semiannual Report, NASA Grant NGR-05-009-030, Nov. 1966.
7. R. Lovberg, Second Semiannual Report, NASA Grant NGR-05-009-030, March 1967.
8. R. Lovberg, Third Semiannual Report, NASA Grant NGR-05-009-030, Nov. 1967.
9. H. R. Griem, Phys. Rev. 131, 1170 (1963).
10. H. N. Olsen, J. Quant. Spectr. Radiative Transfer 3, 59, (1963)..
11. R. H. Garstang, Monthly Notices Roy. Astron. Soc. 114, 118 (1954).
12. H. Statz, F. A. Harrigan, S. H. Koozekanani, C. L. Tang and G. F. Koster, J. Appl. Phys. 36, 2278 (1965).
13. D. Bohm, in The Characteristics of Electrical Discharges in Magnetic Fields, A. Guthrie and R. K. Wakerling, Eds. (McGraw-Hill, New York, 1949).

Figure Captions

- Fig. 1 Plot of $\ln(\lambda I/gA)$ vs. excitation energy for spectral lines of Argon II.
- Fig. 2 Radial arc current density and electron temperature vs. azimuthal distance at a radius of 3.0 cm.
- Fig. 3 Positive directions assumed for components of E , B , v , and J .
- Fig. 4 Sketch of double plane Langmuir probe used in plasma flux measurements.
- Fig. 5 Radial dependence of ion saturation currents to front and rear electrodes of double plane Langmuir probe.
- Fig. 6 Radial arc current density and ion density vs. azimuthal distance at a radius of 3.0 cm.
- Fig. 7 Plasma velocity components vs. azimuthal distance at a radius of 3.0 cm.
- Fig. 8 Radial electric field vs. azimuthal distance at a radius of 3.0 cm. Directly measured values are shown as circles, while calculated values are plotted as triangles.
- Fig. 9 Axial electric field vs. azimuthal distance at a radius of 3.0 cm. Directly measured values are shown as circles, while calculated values are plotted as triangles.
- Fig. 10. Azimuthal electric field vs. azimuthal distance at a radius of 3.0 cm. Directly measured values are shown as circles, while calculated values are plotted as triangles.
- Fig. 11 Flow diagram showing the combinations of observed quantities used to deduce plasma properties. The boxes enclose directly measured quantities, while inferred quantities are enclosed in circles.
- Fig. 12 Schematic drawing of energy analyzer.
- Fig. 13 Output current of energy analyzer as a function of collector voltage. Analyzer positioned 18 cm downstream of anode at a radius of 3.5 cm with its axis parallel to that of the accelerator.
- Fig. 14 Projections of the peak plasma flux and magnetic field on the R- θ and R-Z planes for probe positioned 2 cm downstream of the anode.
- Fig. 15 Projections of the peak plasma flux and magnetic field on the R- θ and R-Z planes for probe positioned 4 cm downstream of the anode.